RESEARCH   **Open Access**

Far-field approximations to the derivatives of Green's function for the Ffowcs Williams and Hawkings equation

Zhiteng Zhou[1,2], Zhenyu Zang[1,2], Hongping Wang[1,2] and Shizhao Wang[1,2]*

*Correspondence:
wangsz@lnm.imech.ac.cn
[1]Institute of Mechanics, Chinese Academy of Sciences, 100190 Beijing, China
Full list of author information is available at the end of the article

Abstract

The surface correction to the quadrupole source term of the Ffowcs Williams and Hawkings integral in the frequency domain suffers from the computation of high-order derivatives of Green's function. The far-field approximations to the derivatives of Green's function have been used without derivation and verification in previous work. In this work, we provide the detailed derivations of the far-field approximations to the derivatives of Green's function. The binomial expansions for the derivatives of Green's function and the far-field condition are employed during the derivations to circumvent the difficulties in computing the high-order derivatives. The approximations to the derivatives of Green's function are systemically verified by using the benchmarks two-dimensional convecting vortex and the co-rotating vortex pair. In addition, we provide the derivations of the approximations to the multiple integrals of Green's function by using the far-field approximations to the derivatives.

Keywords: Ffowcs Williams and Hawkings integral, Green's function, High-order derivatives, Far-field approximation

1 Introduction

The objective of this work is to provide the detailed derivations of the far-field approximations to the derivatives of Green's function for the Ffowcs Williams and Hawkings (FW-H) equation [1]. The FW-H equation is among the most popular acoustic analogy methods to predict sound generated by unsteady flows. The solution to the FW-H equation is usually expressed as an integral over the sources. The integral or the correction to the integral suffers from the computation of derivatives of the Green's function. The far-field approximations to the derivatives of Green's function is a feasible way to circumvent the difficulties in computing the derivatives. The FW-H equation has been successfully used to predict the sound generated by flows from jet engines [2, 3], propellers [4], hydrofoils [5], high-speed trains [6, 7], ducted tail rotors [8] and biomimetic asymmetric bars [9]. The FW-H equation is a nonhomogeneous wave equation that extends Lighthill's acoustic analogy to problems with arbitrarily moving permeable/nonpermeable boundaries. The FW-H equation with a uniform convective flow can be given as follows [10],

$$\left(\frac{1}{c_o^2}\frac{\partial^2}{\partial t^2} + M_iM_j\frac{\partial^2}{\partial x_i\partial x_j} + 2M_i\frac{\partial^2}{\partial x_i\partial t} - \frac{\partial^2}{\partial x_i\partial x_i}\right)\left(H(f)c_o^2\rho'\right)$$
$$= \frac{\partial^2}{\partial x_i\partial x_j}\left(T_{ij}H(f)\right) - \frac{\partial}{\partial x_i}\left(F_i\delta(f)\right) + \frac{\partial}{\partial t}(Q\delta(f)), \tag{1}$$

where $\rho' = \rho - \rho_o$ is the density fluctuation. ρ is the density, and ρ_o is the ambient density at the far field. The far field pressure fluctuation $p' = p - p_o$ is $c_o^2\rho'$ in the assumption that the acoustic wave is an isentropic process. p is the pressure, and p_o is the ambient pressure at the far field. We use the superscript $(\cdot)'$ to denote the fluctuation and subscript $(\cdot)_o$ to denote the far-field variable. t is time. x_i $(i = 1, 2, 3)$ are the independent variables in the Cartesian coordinate system defined by $o-x_1x_2x_3$. $M_i = U_i/c_o$ is the freestream Mach number along the $o-x_i$ axis, where U_i is a component of the freestream velocity. c_o is the speed of sound. f is a function that defines the permeable or nonpermeable boundary by $f = 0$. $f(\mathbf{x})$ also satisfies the constraints that f is greater than zero $(f > 0)$ outside the domain enclosed by the boundary $f = 0$ and less than zero $(f < 0)$ inside the domain. $H(f)$ is the Heaviside's step function which is unity where $f > 0$ and zero where $f < 0$. $\delta(f)$ is the Dirac delta function that is zero everywhere except where $f = 0$. $T_{ij} = \rho u_i u_j + P_{ij} - c_o^2\rho'\delta_{ij}$ is the Lighthill stress tensor, where u_i is the fluid velocity component along the $o-x_i$ axis. $P_{ij} = (p - p_o)\delta_{ij} - \tau_{ij}$ is the compressive stress tensor, where $\rho' = \rho - \rho_o$ is the density fluctuation, ρ_o is the far-field density in the ambient medium, δ_{ij} is the Kronecker delta function and τ_{ij} is the viscous stress tensor. $F_i = \left(P_{ij} + \rho(u_i - U_i)(u_j + U_j) + \rho_oU_iU_j\right)n_j$, where n_j is the normal vector of the permeable/nonpermeable surface S_0 defined by $f = 0$. $Q = (\rho(u_i + U_i) - \rho_oU_i)n_i$. The three terms on the right-hand side of the FW-H equation $\frac{\partial}{\partial t}(Q\delta(f))$, $-\frac{\partial}{\partial x_i}\left(F_i\delta(f)\right)$, and $\frac{\partial^2}{\partial x_i\partial x_j}\left(T_{ij}H(f)\right)$ are usually termed monopole sources, dipole sources, and quadrupole sources, respectively. It is noted that Eq. (1) is a general form of the FW-H equation. When the freestream Mach number is $M_i = 0$, Eq. (1) reduces to the classical form of FW-H equation [1, 11] without boundary motions

$$\left(\frac{1}{c_o^2}\frac{\partial^2}{\partial t^2} - \frac{\partial^2}{\partial x_i\partial x_i}\right)\left(H(f)c_o^2\rho'\right) = \frac{\partial^2}{\partial x_i\partial x_j}\left(T_{ij}H(f)\right) - \frac{\partial}{\partial x_i}\left(F_i\delta(f)\right) + \frac{\partial}{\partial t}(Q\delta(f)). \tag{2}$$

The solution to the FW-H equation can be expressed as surface integrals of the monopole source and dipole source and a volume integral of the quadrupole source. Hereinafter, we refer to these integrals as monopole source term, dipole source term, and quadrupole source term, respectively. The quadrupole source term is usually ignored under the assumption that the monopole source term and dipole source term dominate the far-field sound in low Mach number flows [12]. However, recent studies show that ignoring the quadrupole source term may result in significant spurious sound even at relatively low Mach numbers [13, 14]. The spurious sound results from the vortical or entropy waves that pass across the integral surface [15]. Different methods have been proposed to eliminate or suppress the spurious sound [14, 16–18].

One of the most widely used methods for the elimination of spurious sound is the surface correction integral proposed by Wang et al. [19]. The idea of the surface correction integral is to account for the contribution of the quadrupole sources outside the integral domain because spurious sound is generated by the eddies crossing the boundary of the integral domain. With the frozen eddy assumption, the contribution of the quadrupole sources outside the integral domain can be modelled by using the quadrupole source

flux on the boundary of the integral domain. Then, the surface correction integral can be constructed based on the quadrupole source flux accounting for the contributions of the quadrupole sources outside the integral domain. Spurious sound has been eliminated or dramatically reduced by the surface correction integral in the computation of the sound generated by flows over airfoils [19]. However, the surface correction integral requires that the eddies leave the boundary of the integration domain at a nearly constant speed. To improve the surface correction integral proposed by Wang et al. [19], different methods have been proposed based on accounting for the nonconstant convective velocity at the boundary of the integral domain [13, 18]. Most of the surface correction integrals are developed within the time-domain framework.

Lockard and Casper [20] first proposed the surface correction integral for the FW-H equation within the frequency domain. The derivation of the surface correction integral for the frequency-domain method involves repeated integration by parts. Thus, the surface correction integral reported by Lockard and Casper [20] consists of a series of surface integrals as follows

$$I_Q(\mathbf{x};\omega) \approx -\sum_{l=1}^{n} \int_{f=0} \left(\frac{-\mathrm{i}U_1}{\omega} \right)^l T_{ij}(\mathbf{y},\omega) \frac{\partial^{l-1}}{\partial y_1^{l-1}} \left(\frac{\partial^2 G(\mathbf{x};\mathbf{y})}{\partial y_i \partial y_j} \right) dS, \tag{3}$$

where $f = 0$ is the boundary of the volume integral of the quadrupole source in the FW-H equation (hereinafter referred to as the FW-H integral surface). $\mathrm{i} = \sqrt{-1}$ is the unit of the imaginary number. Without loss of generality, we set the convective velocity of the quadrupole sources along the $o - x_1$ direction and use U_1 to denote the convective velocity. $G(\mathbf{x};\mathbf{y})$ is Green's function, where $\mathbf{x}$ and $\mathbf{y}$ are the observer and source positions, respectively. ω is the frequency. The surface correction integral for the frequency-domain method (Eq. (3)) works reasonably well in the test cases of a convecting vortex when the convective Mach number of the flow $M_a = U_1/c_o$ is lower than 0.5. The problems with the surface correction integral for the frequency-domain method (Eq. (3)) are that (1) the series of surface integrals on the right-hand side of Eq. (3) may diverge when the convective Mach number is higher than 0.5, and (2) the computation of the high-order derivatives of Green's function is quite complicated and nontrivial [20]. The divergence of Eq. (3) is caused by the convective velocity larger than the phase velocity of a perturbation propagating through convective flows. The far-field approximations to the derivatives of Green's function have also been utilized to fix the second problem of the surface correction integral. However, these far-field approximations to the derivatives of Green's function have been used without derivation and verification [21].

Detailed derivations and verification of the approximations to the derivatives of Green's function are given in this work. The derivations of the approximations are based on the binomial expansion of the derivatives of Green's function and the far-field condition. These approximations to the derivatives are verified in detail by computing the far-field acoustic pressure from the quadrupole source term generated by the two-dimensional convecting vortex and the co-rotating vortex pair. In addition, the approximations to the integrals of Green's function are derived by using the approximations to the derivatives of Green's function.

The remainder of the paper is organized as follows. We will give the derivations of the approximations to the derivatives of Green's function for 2D and 3D flows in Section 2.

The verifications of the approximations to the derivatives of Green's function are reported in Section 3. Finally, conclusions are drawn in Section 4.

2　Far-field approximations to the derivatives of Green's function

We investigate the FW-H equation in the form of a convective wave equation in the frequency domain in accordance with the work of Lockard et al. [10, 20]. Green's function for the convective wave equation in the frequency domain is simply referred to as Green's function hereinafter when there is no ambiguity. We directly give the expressions of the far-field approximations to the derivatives of Green's function in subsection 2.1. Then, we provide the detailed derivations of the approximations in subsection 2.2.

2.1　Expressions of the far-field approximations to the derivatives of Green's function

The $(l+2)$th-order derivative of Green's function with respect to the variables y_q, y_i and y_j can be approximated at the far field as follows:

$$\frac{\partial^l}{\partial y_q^l}\left(\frac{\partial^2 G(\mathbf{x};\mathbf{y})}{\partial y_i \partial y_j}\right) \approx \left(\frac{\partial \varphi(\mathbf{x};\mathbf{y})}{\partial y_q}\right)^l \frac{\partial^2 G(\mathbf{x};\mathbf{y})}{\partial y_i \partial y_j}, \tag{4}$$

where G is Green's function and φ is the phase function of Green's function.

For the two-dimensional (2D) flows, we have $G \approx G_{2D}$ and $\varphi = \varphi_{2D}$ in the far field with

$$G_{2D} = \frac{i}{4\beta}\left(\frac{2\beta^2}{\pi k R}\right)^{\frac{1}{2}} \exp^{\varphi_{2D}}, \tag{5}$$

$$\varphi_{2D}(\mathbf{x};\mathbf{y}) = i\left[\frac{Mk(x_1 - y_1)}{\beta^2} + \frac{\pi}{4} - \frac{k}{\beta^2}R\right], \tag{6}$$

where the observer and source locations are denoted by $\mathbf{x}$ and $\mathbf{y}$, respectively. $k = \omega/c_o$ is the wavenumber. $\beta = \sqrt{1 - M^2}$ is the Prantle-Glauert factor. M is the Mach number of the freestream flow. The distance R is computed by

$$R = R_{2D} = \sqrt{(x_1 - y_1)^2 + \beta^2(x_2 - y_2)^2}. \tag{7}$$

It is noted that the 2D Green's function G_{2D} given in Eq. (5) is the asymptotic Green's function for 2D flows.

For the three-dimensional (3D) flows, we have $G = G_{3D}$ and $\varphi = \varphi_{3D}$ with

$$G_{3D} = -\frac{1}{4\pi R}\exp^{\varphi_{3D}}, \tag{8}$$

$$\varphi_{3D}(\mathbf{x};\mathbf{y}) = -ik\frac{(R - M(x_1 - y_1))}{\beta^2}, \tag{9}$$

where the distance R is computed by

$$R = R_{3D} = \sqrt{(x_1 - y_1)^2 + \beta^2(x_2 - y_2)^2 + \beta^2(x_3 - y_3)^2}. \tag{10}$$

By using the approximations to the derivatives to Green's function (Eq. (4)), the surface correction integral (Eq. (3)) proposed by Lockard and Casper [20] can be approximated by

$$I_Q(\mathbf{x};\omega) \approx -\sum_{l=1}^{n}\int_{f=0}\left(\frac{U_1}{i\omega}\right)^l T_{ij}(\mathbf{y},\omega)\left(\frac{\partial \varphi(\mathbf{x};\mathbf{y})}{\partial y_1}\right)^{l-1}\frac{\partial^2 G(\mathbf{x};\mathbf{y})}{\partial y_i \partial y_j}dS. \tag{11}$$

The high-order derivatives of Green's function $\frac{\partial^{l-1}}{\partial y_1^{l-1}}\left(\frac{\partial^2 G(\mathbf{x};\mathbf{y})}{\partial y_i \partial y_j}\right)$ in Eq. (3) are approximated by $\left(\frac{\partial \varphi(\mathbf{x};\mathbf{y})}{\partial y_1}\right)^{l-1}\frac{\partial^2 G(\mathbf{x};\mathbf{y})}{\partial y_i \partial y_j}$ in Eq. (11). Therefore, the difficulties in computing the high-order derivatives of Green's function are circumvented.

2.2 Derivations of the approximations to the derivatives of Green's function at the far field

The approximations in Eq. (4) can be derived separately by setting $q = 1, \cdots, N_D$, where $N_D = 2$ for two-dimensional flows and $N_D = 3$ for three-dimensional flows. We report the detailed derivation of the approximations to the derivatives of Green's function when $q = 1$ in Eq. (4). The same derivations can be obtained following the same method for $q = 2$ and $q = 3$. The subscript $q = 1$ in Eq. (4) indicates that the lth-order derivative of $\frac{\partial^2 G(\mathbf{x};\mathbf{y})}{\partial y_i \partial y_j}$ is taken along the direction of the $o - y_1$ axis. When the subscript $q = 1$, Eq. (4) can be expressed as

$$\frac{\partial^l}{\partial y_1^l}\left(\frac{\partial^2 G(\mathbf{x};\mathbf{y})}{\partial y_i \partial y_j}\right) \approx \left(\frac{\partial \varphi(\mathbf{x};\mathbf{y})}{\partial y_1}\right)^l \frac{\partial^2 G(\mathbf{x};\mathbf{y})}{\partial y_i \partial y_j}. \tag{12}$$

We re-write the left-hand-side of Eq. (12) as

$$\frac{\partial^l}{\partial y_1^l}\left(\frac{\partial^2 G(\mathbf{x};\mathbf{y})}{\partial y_i \partial y_j}\right) = \frac{\partial^2}{\partial y_i \partial y_j}\left(\frac{\partial^l G(\mathbf{x};\mathbf{y})}{\partial y_1^l}\right). \tag{13}$$

For the two-dimensional flows with $G = G_{2D}$, the lth-order derivative of Green's function with respect to the variable y_1 can be expressed with the binomial expansion as follows

$$\frac{\partial^l G_{2D}(\mathbf{x};\mathbf{y})}{\partial y_1^l} = \frac{i}{4\beta}\left(\frac{2\beta^2}{\pi k}\right)^{1/2}\sum_{k_1=0}^{l} C_l^{k_1}\frac{\partial^{k_1}\exp^{\varphi(\mathbf{x};\mathbf{y})}}{\partial y_1^{k_1}}\frac{\partial^{l-k_1}(R^{-1/2})}{\partial y_1^{l-k_1}}, \tag{14}$$

where $C_l^{k_1}$ is the binomial coefficient.

We consider the far-field sound generated by the compact source flows. Without loss of generality, we set the origin of the reference frame near the compact source flows. For the far-field sound at the observation position $\mathbf{x}$ generated by the sources at the position $\mathbf{y}$, we have $|\mathbf{x}| \gg |\mathbf{y}|$. The k_1th-order derivative to the distance R given by Eqs. (7) and (10) can be approximated by

$$\frac{\partial^{k_1} R}{\partial y_1^{k_1}} \approx O\left(R^{-k_1}\right)R. \tag{15}$$

Similarly, we have

$$\frac{\partial^{k_1}(R^{-1/2})}{\partial y_1^{k_1}} \approx O\left(R^{-k_1}\right)R^{-1/2}. \tag{16}$$

The detailed derivations of Eqs. (15) and (16) are reported in Appendix B. By using Eq. (15), the k_1th-order derivative of $\exp^{\varphi(\mathbf{x};\mathbf{y})}$ can be approximated by

$$\frac{\partial^{k_1}\exp^{\varphi(\mathbf{x};\mathbf{y})}}{\partial y_1^{k_1}} \approx \left(\frac{\partial \varphi(\mathbf{x};\mathbf{y})}{\partial y_1}\right)^{k_1}\exp^{\varphi(\mathbf{x};\mathbf{y})}(k_1 \geq 1). \tag{17}$$

The detailed derivation of Eq. (17) is reported in Appendix C. Thus, the binomial expansion of Eq. (5) can be expressed as

$$\frac{\partial^l G_{2D}(\mathbf{x};\mathbf{y})}{\partial y_1^l} = \frac{i}{4\beta}\left(\frac{2\beta^2}{\pi k}\right)^{1/2}\sum_{k_1=0}^{l} C_l^{k_1}\frac{\partial^{k_1}\exp^{\varphi(\mathbf{x};\mathbf{y})}}{\partial y_1^{k_1}}\frac{\partial^{l-k_1}(R^{-1/2})}{\partial y_1^{l-k_1}}$$
$$\approx \frac{i}{4\beta}\left(\frac{2\beta^2}{\pi k}\right)^{1/2}\sum_{k_1=0}^{l} C_l^{k_1}\left(\frac{\partial\varphi(\mathbf{x};\mathbf{y})}{\partial y_1}\right)^{k_1}\exp^{\varphi(\mathbf{x};\mathbf{y})}\frac{\partial^{l-k_1}(R^{-1/2})}{\partial y_1^{l-k_1}}. \tag{18}$$

Furthermore, the derivatives of $R^{-1/2}$ terms on the right-hand side of Eq. (18) can be approximated according to Eq. (16). Thus, we obtain the far-field approximations to the $(l+2)$th-order derivatives of Green's function for the two-dimensional flows with $q=1$ as follows

$$\frac{\partial^l}{\partial y_1^l}\left(\frac{\partial^2 G_{2D}(\mathbf{x};\mathbf{y})}{\partial y_i\partial y_j}\right) \approx \left(\frac{\partial\varphi_{2D}(\mathbf{x};\mathbf{y})}{\partial y_1}\right)^l\frac{\partial^2 G_{2D}(\mathbf{x};\mathbf{y})}{\partial y_i\partial y_j}. \tag{19}$$

For three-dimensional flows with $G=G_{3D}$, the lth-order derivative of Green's function with respect to the variable y_1 can be expressed with the binomial expression as follows

$$\frac{\partial^l G_{3D}(\mathbf{x};\mathbf{y})}{\partial y_1^l} = \frac{-1}{4\pi}\sum_{k_1=0}^{l} C_l^{k_1}\frac{\partial^{k_1}\exp^{\varphi(\mathbf{x};\mathbf{y})}}{\partial y_1^{k_1}}\frac{\partial^{l-k_1}(R^{-1})}{\partial y_1^{l-k_1}}. \tag{20}$$

It is noted that Eq. (19) is not directly obtained from Eq. (18). A second-order derivative of Eq. (18) is first derived. Then, according to Eq. (16) and Appendix C, Eq. (19) can be obtained by ignoring the terms of high-order of $R^{-1/2}$ and φ.

For the far-field sound at the observation position $\mathbf{x}$ generated by the sources at the position $\mathbf{y}$, we have $|\mathbf{x}| \gg |\mathbf{y}|$. The approximated k_1th-order derivative to the distance R given by Eq. (15) is then employed to give the three-dimensional formulation of Eq. (17). Therefore, the binomial expansion as Eq. (20) can be expressed as

$$\frac{\partial^l G_{3D}(\mathbf{x};\mathbf{y})}{\partial y_1^l} = \frac{-1}{4\pi}\sum_{k_1=0}^{l} C_l^{k_1}\left(\frac{\partial\varphi(\mathbf{x};\mathbf{y})}{\partial y_1}\right)^{k_1}\exp^{\varphi(\mathbf{x};\mathbf{y})}\frac{\partial^{l-k_1}(R^{-1})}{\partial y_1^{l-k_1}}$$
$$\approx \frac{-1}{4\pi}\sum_{k_1=0}^{l} C_l^{k_1}\left(\frac{\partial\varphi(\mathbf{x};\mathbf{y})}{\partial y_1}\right)^{k_1}\exp^{\varphi(\mathbf{x};\mathbf{y})}\frac{\partial^{l-k_1}(R^{-1})}{\partial y_1^{l-k_1}}. \tag{21}$$

Similar to the derivation of Eq. (15), the k_1th-order derivative of R^{-1} can be approximated as follows

$$\frac{\partial^{k_1}(R^{-1})}{\partial y_1^{k_1}} \approx O\left(R^{-k_1}\right)R^{-1}. \tag{22}$$

Furthermore, the approximated derivatives of R^{-1} terms can be employed to simplify the right-hand side of Eq. (21). Thus, we obtain the far-field approximations to the $(l+2)$th-order derivative of Green's function for the three-dimensional flows with $q=1$ as follows

$$\frac{\partial^l}{\partial y_1^l}\left(\frac{\partial^2 G_{3D}(\mathbf{x};\mathbf{y})}{\partial y_i\partial y_j}\right) \approx \left(\frac{\partial\varphi_{3D}(\mathbf{x};\mathbf{y})}{\partial y_1}\right)^l\frac{\partial^2 G_{3D}(\mathbf{x};\mathbf{y})}{\partial y_i\partial y_j}. \tag{23}$$

The full derivations of the approximations given by Eq. (4) can be obtained by setting the subscript $q=2$ for two-dimensional flows and $q=2,3$ for three-dimensional flows.

3   Results and discussion

We verify the proposed esimations by the benchmark cases of two-dimensional convect-
ing vortex and co-rotating vortex pair. It is noted that both the benchmark cases reported
in this section can be addressed by using the classical FW-H solver. Here, we have used
different methods to solve the two benchmark cases to verify the formulations proposed
in this manuscript.

3.1   Two-dimensional convecting vortex

We use the benchmark flow of a two-dimensional convecting vortex to verify the approx-
imations to the derivatives of Green's function in this subsection. The time-varying
velocity and pressure of the convecting vortex are given by:

$$
\begin{aligned}
p &= \frac{1}{\gamma}\left(1 - a_2 \exp\left(1 - r^2\right)\right)^{\frac{\gamma}{\gamma-1}}, \\
u &= U_1 - a_0 a_1 y_2 \exp\left(\left(1 - r^2\right)/2\right), \\
v &= a_0 a_1 (y_1 - M_a t) \exp\left(\left(1 - r^2\right)/2\right), \\
\rho &= \left(\frac{p}{p_o}\right)^{1/\gamma},
\end{aligned}
\tag{24}
$$

where p_o is the pressure of the ambient medium at the far field. $\gamma = 1.4$ is the specific
heat ratio of air. The quantities are normalized by using the ambient speed of sound c_o,
reference length L and density ρ of fluid. We assume that the vortex is convected along
the $o - y_1$ axis with a velocity of U_1. $M_a = U_1/c_o$ is the convecting Mach number, which
is equal to the freestream Mach number. The parameters are given by $a_0 = 1$ and $a_1 = 1/(2\pi)$, respectively. The parameters a_2 and r are computed by

$$
\begin{aligned}
a_2 &= (\gamma - 1)a_0^2 a_1^2/2, \\
r^2 &= (y_1 - M_a t)^2 + y_2^2.
\end{aligned}
\tag{25}
$$

Figure 1 gives the schematic of the pressure field when the two-dimensional convecting
vortex crosses the permeable FW-H integral surface. Here, we take the permeable FW-H
integral surface as a square with an edge of 10 units in length, as shown by the dashed
edges in Fig. 1. The contours in Fig. 1 show the distribution of the fluctuating pressure
$p - p_o$, which is normalized by p_o.

The pressure fluctuation approaches zero monotonically away from the vortex centre,
as shown in Fig. 2, where the convecting Mach number of the vortex is $M_a = 0.2$. Thus,
the sound pressure should approach zero at the far field [17]. However, the computation
of the far-field sound pressure using the FW-H integral without the surface correction
results in significant spurious sound when the vortex is moving across the permeable
integral surface, as shown in Fig. 3, where the solid line shows the acoustic pressure com-
puted by using the FW-H surface integral at the position $\mathbf{x} = (100, 0)$ that is completely
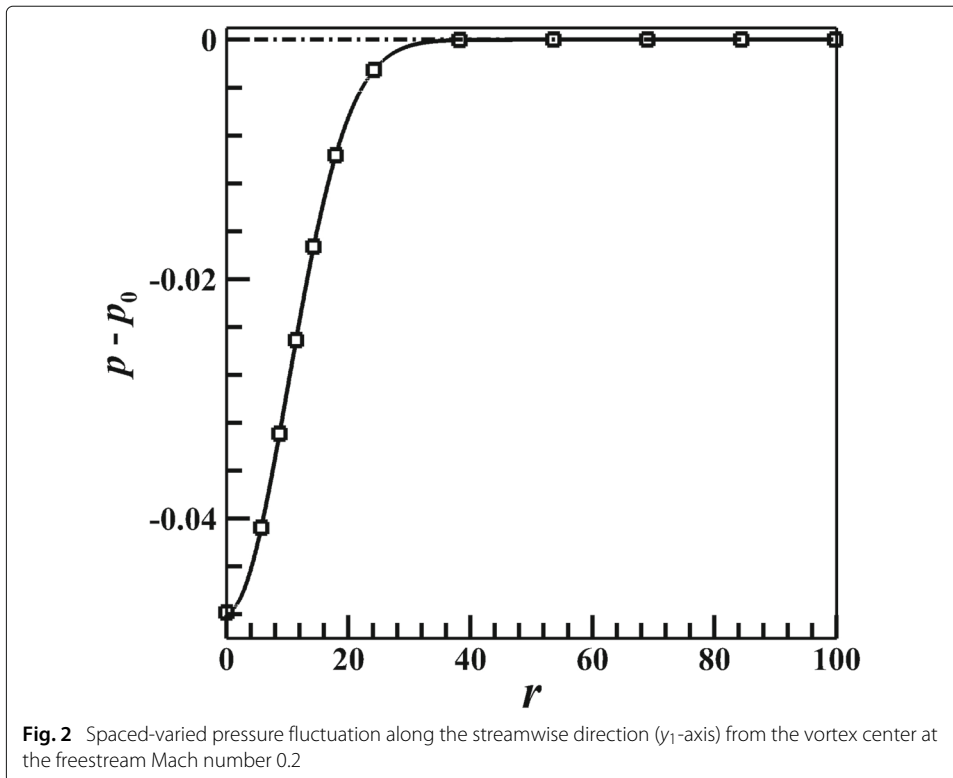spurious sound.

The surface correction integral given by Eq. (3) and its approximation at the far field
given by Eq. (11) are shown by dashed lines and dash-dotted lines in Fig. 3, respectively.
For convenient comparison, we plot the minus of the surface correction integral, i.e., $-I_Q$,
in Fig. 3. It is clear that the surface correction integrals computed with both the origi-
nal derivatives of Green's function (Eq. (3)) and the approximated derivatives of Green's
function (Eq. (11)) can accurately estimate the spurious sound generated by the vortex

Fig. 1 Instantaneous pressure fluctuation field generated by a convecting vortex
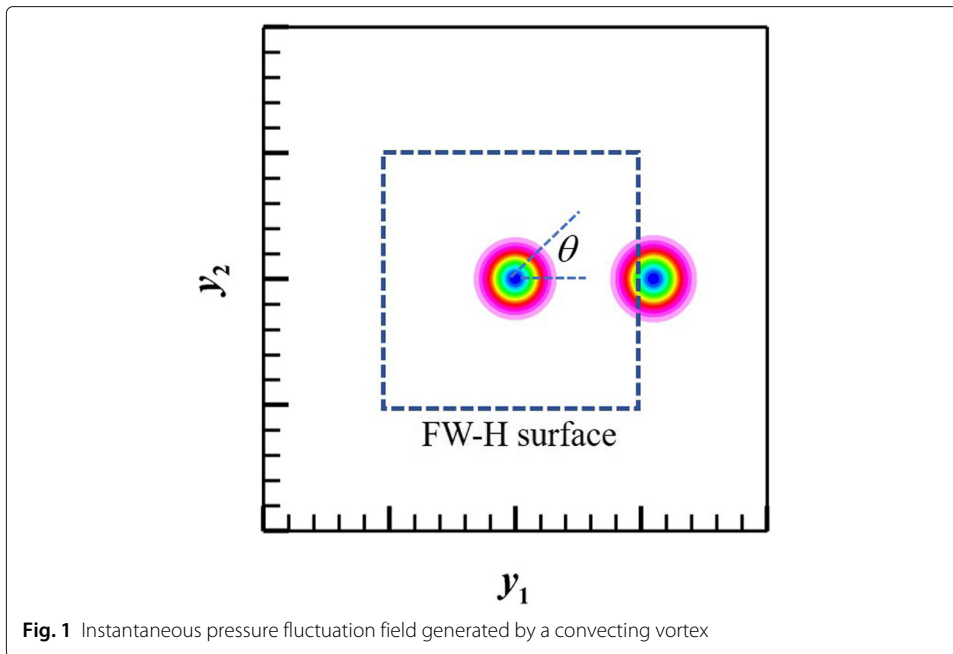
crossing the integral surface. The results shown in Fig. 3 indicate that the approximations of Eq. (4) are correct. To further verify the approximations to the derivatives of Green's function, we compare the first three terms in Eqs. (3) and (11) in detail as follows.

We denote the first, second and third terms in Eq. (3) by

$$p_1'(\mathbf{x}; \omega) = -\int_{f=0} \left(\frac{-iU_1}{\omega} \right) T_{ij}(\mathbf{y}, \omega) \left(\frac{\partial^2 G(\mathbf{x}; \mathbf{y})}{\partial y_i \partial y_j} \right) dS, \tag{26}$$
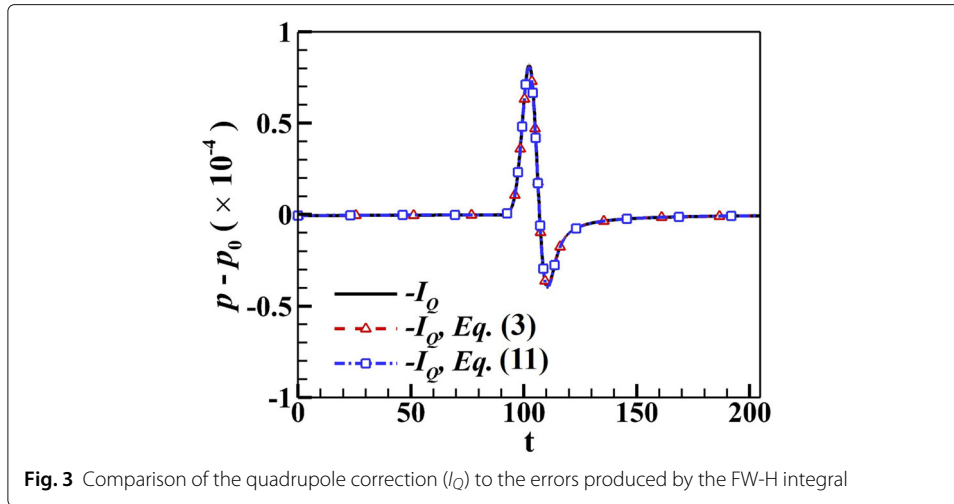

Fig. 2 Spaced-varied pressure fluctuation along the streamwise direction (y_1-axis) from the vortex center at the freestream Mach number 0.2

Fig. 3 Comparison of the quadrupole correction (I_Q) to the errors produced by the FW-H integral

$$p_2'(\mathbf{x};\omega) = -\int_{f=0} \left(\frac{-iU_1}{\omega}\right)^2 T_{ij}(\mathbf{y},\omega)\frac{\partial}{\partial y_1}\left(\frac{\partial^2 G(\mathbf{x};\mathbf{y})}{\partial y_i \partial y_j}\right)\mathrm{d}S, \tag{27}$$

$$p_3'(\mathbf{x};\omega) = -\int_{f=0} \left(\frac{-iU_1}{\omega}\right)^3 T_{ij}(\mathbf{y},\omega)\frac{\partial^2}{\partial y_1^2}\left(\frac{\partial^2 G(\mathbf{x};\mathbf{y})}{\partial y_i \partial y_j}\right)\mathrm{d}S, \tag{28}$$

and the first, second and third terms in Eq. (11) by

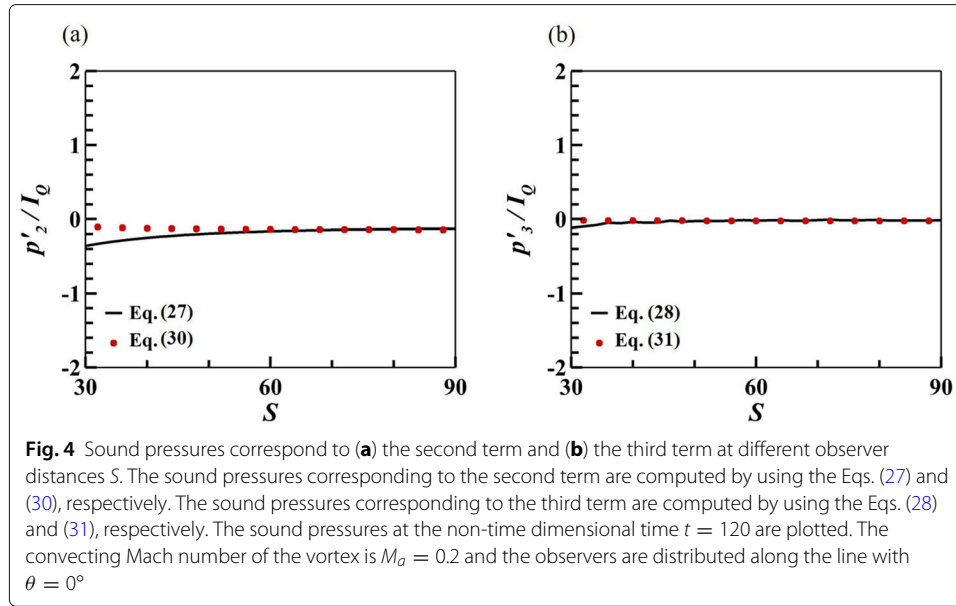$$p_{1,\mathrm{appr}}'(\mathbf{x};\omega) = -\int_{f=0} \left(\frac{-iU_1}{\omega}\right) T_{ij}(\mathbf{y},\omega)\left(\frac{\partial^2 G(\mathbf{x};\mathbf{y})}{\partial y_i \partial y_j}\right)\mathrm{d}S, \tag{29}$$

$$p_{2,\mathrm{appr}}'(\mathbf{x};\omega) = -\int_{f=0} \left(\frac{-iU_1}{\omega}\right)^2 T_{ij}(\mathbf{y},\omega)\frac{\partial\varphi}{\partial y_1}\left(\frac{\partial^2 G(\mathbf{x};\mathbf{y})}{\partial y_i \partial y_j}\right)\mathrm{d}S, \tag{30}$$

$$p_{3,\mathrm{appr}}'(\mathbf{x};\omega) = -\int_{f=0} \left(\frac{-iU_1}{\omega}\right)^3 T_{ij}(\mathbf{y},\omega)\left(\frac{\partial\varphi}{\partial y_1}\right)^2\left(\frac{\partial^2 G(\mathbf{x};\mathbf{y})}{\partial y_i \partial y_j}\right)\mathrm{d}S, \tag{31}$$
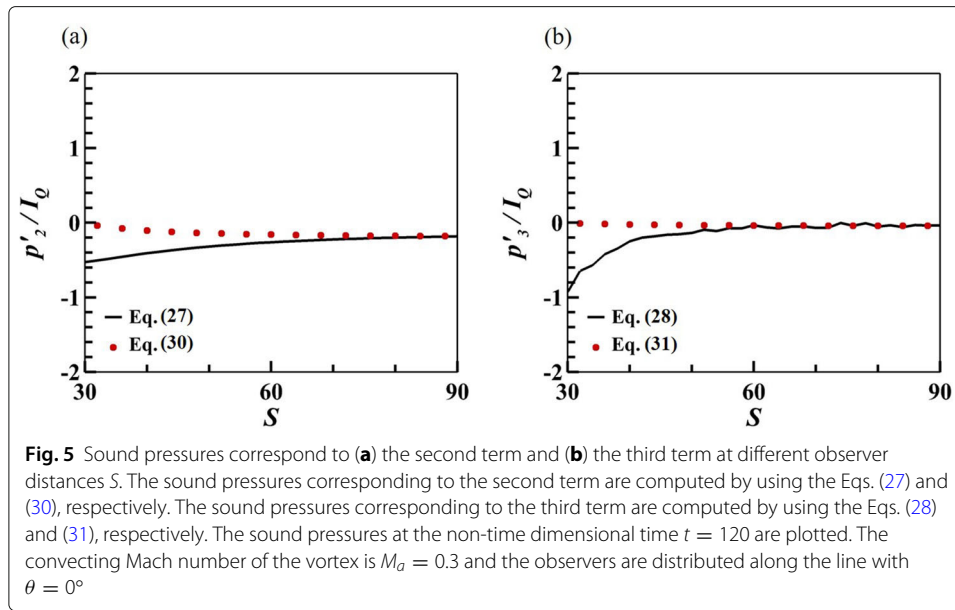
where we use the subscript "appr" to indicate the approximated computation of the derivatives of Green's function in Eq. (11). The first terms in Eq. (3) and Eq. (11) are exactly the same since the approximation to the derivative of Green's function is not used. The differences between the second and third terms in Eq. (3) and Eq. (11) are that the approximations to the derivatives of Green's function are used in Eq. (11), as shown in Eqs. (27), (30) and (28), (31), respectively. We verify the approximations to the derivatives of Green's function by comparing the second terms (Eqs. (27), (30)) and the third terms (Eqs. (28), (31)) at different observer distances, different directions, and different convecting Mach numbers.

Figure 4 shows the sound pressures corresponding to the second and third terms at different observer distances $S = |\mathbf{x} - \mathbf{Y_0}|$, where $\mathbf{x}$ and $\mathbf{Y_0}$ are the observer position and the initial central position of the convecting vortex, respectively. We set the initial central position of the convecting vortex at $\mathbf{Y_0} = \mathbf{0}$ in this work. The central position of the convecting vortex $\mathbf{Y}$ moves along the $o - y_1$ axis. The sound pressures at the non-time dimensional time $t = 120$ are plotted in Fig. 4. At this time moment of $t = 120$, the central position of the convecting vortex is at $\mathbf{Y} = (24.0, 0.0)$. For the case reported in Fig. 4, the convecting Mach number of the vortex is $M_a = 0.2$, and the observers are distributed along the line with $\theta = 0°$, where θ is defined as the angle between the observer position

Fig. 4 Sound pressures correspond to (**a**) the second term and (**b**) the third term at different observer distances S. The sound pressures corresponding to the second term are computed by using the Eqs. (27) and (30), respectively. The sound pressures corresponding to the third term are computed by using the Eqs. (28) and (31), respectively. The sound pressures at the non-time dimensional time $t = 120$ are plotted. The convecting Mach number of the vortex is $M_a = 0.2$ and the observers are distributed along the line with $\theta = 0°$
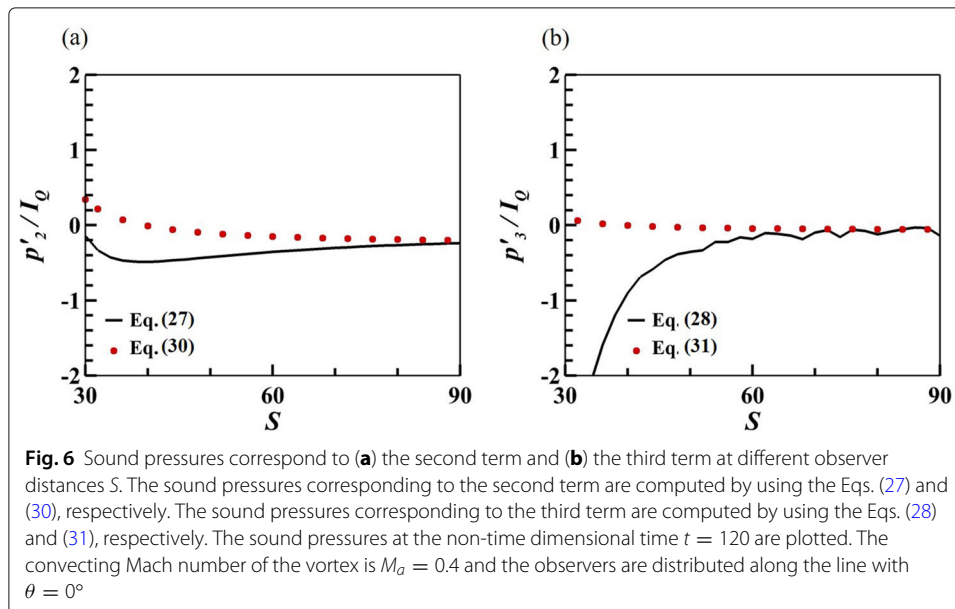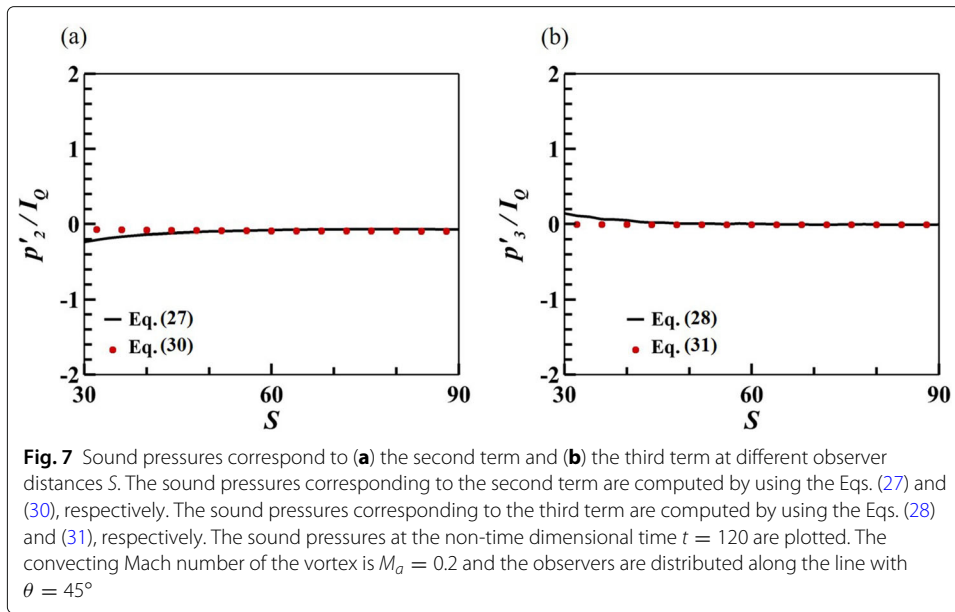
and the $o - y_1$ axis, as shown in Fig. 1. The variations in the sound pressure computed by using Eqs. (27) and (30) are shown in Fig. 4(a). The results indicate that the sound pressure $p'_{2,\text{appr}}$ approaches the sound pressure p'_2 as the observer distance S increases. The difference between the sound pressure $p'_{2,\text{appr}}$ and p'_2 is less than 5% of $I_Q(\mathbf{x})$ at the same position when $S > 53$, indicating that the right-hand side of Eq. (4) gives a reasonable approximation to its left-hand side when $l = 1$ when the observer distance $S > 53$. The variations in the sound pressure computed by using Eqs. (28) and (31) are shown in Fig. 4(b). Similar to that corresponding to the second term, the sound pressure $p'_{3,\text{appr}}$ approaches the sound pressure p'_3 as the observer distance S increases. The difference between the sound pressure $p'_{3,\text{appr}}$ and p'_3 is less than 5% of $I_Q(\mathbf{x})$ at the same position when $S > 35$, indicating that the right-hand side of Eq. (4) gives a reasonable approximation to its left-hand side when $l = 2$ when the observer distance $S > 35$. The results also indicate that the approximation on the left-hand side of Eq. (4) converges to its right-hand side faster with $l = 2$ than that with $l = 1$.

Figures 5 and 6 show the variations in the sound pressures with the observer distances at convecting Mach numbers of $M_a = 0.3$ and $M_a = 0.4$, respectively. The observers are distributed along the line with $\theta = 0°$. We plot the sound pressures at the same non-time dimensional time $t = 120$ as the case in Fig. 4. At time $t = 120$, the central position of the convecting vortex is at $\mathbf{Y} = (36.0, 0.0)$ for $M_a = 0.3$ and $\mathbf{Y} = (48.0, 0.0)$ for $M_a = 0.4$. For $M_a = 0.3$, the variations in the sound pressure computed by using Eqs. (27) and (30) are shown in Fig. 5(a). Similar to Fig. 4(a), the sound pressure $p'_{2,\text{appr}}$ approaches the sound pressure p'_2 as the observer distance S increases. The difference between the sound pressure $p'_{2,\text{appr}}$ and p'_2 is less than 5% of $I_Q(\mathbf{x})$ at the same position when $S > 71$. The variations in the sound pressure computed by using Eqs. (28) and (31) are shown in Fig. 5(b). The sound pressure $p'_{3,\text{appr}}$ approaches the sound pressure p'_3 as the observer distance S increases. The difference between the sound pressure $p'_{3,\text{appr}}$ and p'_3 is less than 5% of $I_Q(\mathbf{x})$ at the same position when $S > 56$. The results also support the conclusion that the approximation on the left-hand side of Eq. (4) approaches its right-hand side more rapidly with $l = 2$ than with $l = 1$. Compared with those plotted in Fig. 4, the

Fig. 5 Sound pressures correspond to (**a**) the second term and (**b**) the third term at different observer distances S. The sound pressures corresponding to the second term are computed by using the Eqs. (27) and (30), respectively. The sound pressures corresponding to the third term are computed by using the Eqs. (28) and (31), respectively. The sound pressures at the non-time dimensional time $t = 120$ are plotted. The convecting Mach number of the vortex is $M_a = 0.3$ and the observers are distributed along the line with $\theta = 0°$
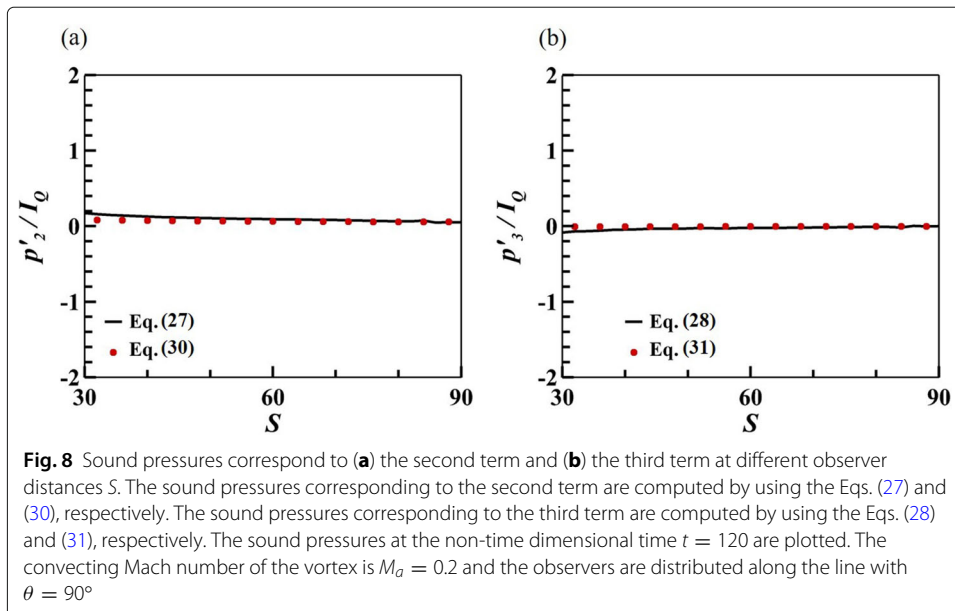
results indicate that the approximations on the left-hand side of Eq. (4) approach its right-hand side more slowly for $M_a = 0.3$ than for $M_a = 0.2$. For $M_a = 0.4$, the variations in the sound pressure computed by using Eqs. (27) and (30) are shown in Fig. 6(a). Similar to those plotted in Figs. 4(a) and 5(a), the sound pressure $p'_{2,\text{appr}}$ approaches the sound pressure p'_2 as the observer distance S increases. The variations in the sound pressure computed by using Eqs. (28) and (31) are shown in Figure 6(b). The sound pressure $p'_{3,\text{appr}}$ approaches the sound pressure p'_3 as the observer distance S increases. All of these results support the conclusion that the approximation on the left-hand side of Eq. (4) converges to its right-hand side faster with $l = 2$ than that with $l = 1$. Compared with the plots in Figs. 4 and 5, the results also indicate that the convergence of approximations on the left-hand side of Eq. (4) to its right-hand side becomes slow as the convecting Mach number increases.

Fig. 6 Sound pressures correspond to (**a**) the second term and (**b**) the third term at different observer distances S. The sound pressures corresponding to the second term are computed by using the Eqs. (27) and (30), respectively. The sound pressures corresponding to the third term are computed by using the Eqs. (28) and (31), respectively. The sound pressures at the non-time dimensional time $t = 120$ are plotted. The convecting Mach number of the vortex is $M_a = 0.4$ and the observers are distributed along the line with $\theta = 0°$

Fig. 7 Sound pressures correspond to (**a**) the second term and (**b**) the third term at different observer distances S. The sound pressures corresponding to the second term are computed by using the Eqs. (27) and (30), respectively. The sound pressures corresponding to the third term are computed by using the Eqs. (28) and (31), respectively. The sound pressures at the non-time dimensional time $t = 120$ are plotted. The convecting Mach number of the vortex is $M_a = 0.2$ and the observers are distributed along the line with $\theta = 45°$

Figures 7 and 8 show the variations in the sound pressures with the observer distances along the directions with $\theta = 45°$ and $\theta = 90°$, respectively. The convecting Mach number is set as $M_a = 0.2$. We plot the sound pressures at the same non-time dimensional time $t = 120$ as that for the case shown in Fig. 4. For $\theta = 45°$, the variations in the sound pressure computed by using Eqs. (27) and (30) are shown in Fig. 7(a). Similar to those plotted in Fig. 4(a), the sound pressure $p'_{2,\text{appr}}$ converges to the sound pressure p'_2 as the observer distance S increases. The difference between the sound pressure $p'_{2,\text{appr}}$ and p'_2 is less than 5% of $I_Q(\mathbf{x})$ at the same position when $S > 42$. The variations in the sound pressure computed by using Eqs. (28) and (31) are shown in Fig. 7(b). The sound pressure $p'_{3,\text{appr}}$ converges to the sound pressure p'_3 as the observer distance S increases. The difference between the sound pressure $p'_{3,\text{appr}}$ and p'_3 is less than 5% of $I_Q(\mathbf{x})$ at the same position when $S > 39$. For $\theta = 90°$, the variations in the sound pressure computed by

Fig. 8 Sound pressures correspond to (**a**) the second term and (**b**) the third term at different observer distances S. The sound pressures corresponding to the second term are computed by using the Eqs. (27) and (30), respectively. The sound pressures corresponding to the third term are computed by using the Eqs. (28) and (31), respectively. The sound pressures at the non-time dimensional time $t = 120$ are plotted. The convecting Mach number of the vortex is $M_a = 0.2$ and the observers are distributed along the line with $\theta = 90°$

using Eqs. (27) and (30) are shown in Fig. 8(a). The sound pressure $p'_{2,\text{appr}}$ converges to the sound pressure p'_2 as the observer distance S increases. The difference between the sound pressure $p'_{2,\text{appr}}$ and p'_2 is less than 5% of $I_Q(\mathbf{x})$ at the same position when $S > 42$. The variations in the sound pressure computed by using Eqs. (28) and (31) are shown in Fig. 8(b). The sound pressure $p'_{3,\text{appr}}$ converges to the sound pressure p'_3 as the observer distance S increases. The difference between the sound pressure $p'_{3,\text{appr}}$ and p'_3 is less than 5% of $I_Q(\mathbf{x})$ at the same position when $S > 37$. All of these results support the conclusion that the approximation on the left-hand side of Eq. (4) converges to its right-hand side faster with $l = 2$ than that with $l = 1$. Comparison of the results plotted in Figures 4, 7, and 8 indicates that the approximations on the left-hand side of Eq. (4) converge to its right-hand side and become faster as the directive angle θ increases.

3.2　Co-rotating vortex pair

In this subsection, we use the benchmark flow of a co-rotating vortex pair to verify the approximations to the derivatives of Green's function. The co-rotating vortex pair is a classical model for studying the jet engine noise generated from the interaction of coherent structures [22]. A co-rotating vortex pair can be modelled by two line vortices of equal strength separated by the distance $2d$, as shown in Fig. 9 [23]. The sound generated by the co-rotating vortex pair can be computed by modifying Lighthill's acoustic analogy equation into the vortex sound equation as follows

$$\frac{1}{c_\infty^2}\frac{\partial^2 p'}{\partial t^2} - \frac{\partial^2 p'}{\partial x_i^2} = \rho_0 \frac{\partial(\omega \times \mathbf{v})_i}{\partial x_i}, \tag{32}$$

where the sound sources other than the divergence of the Lamb vector $\omega \times \mathbf{v}$ are neglected according to dimensional analysis [24]. The corresponding frequency-domain formulation can be expressed as
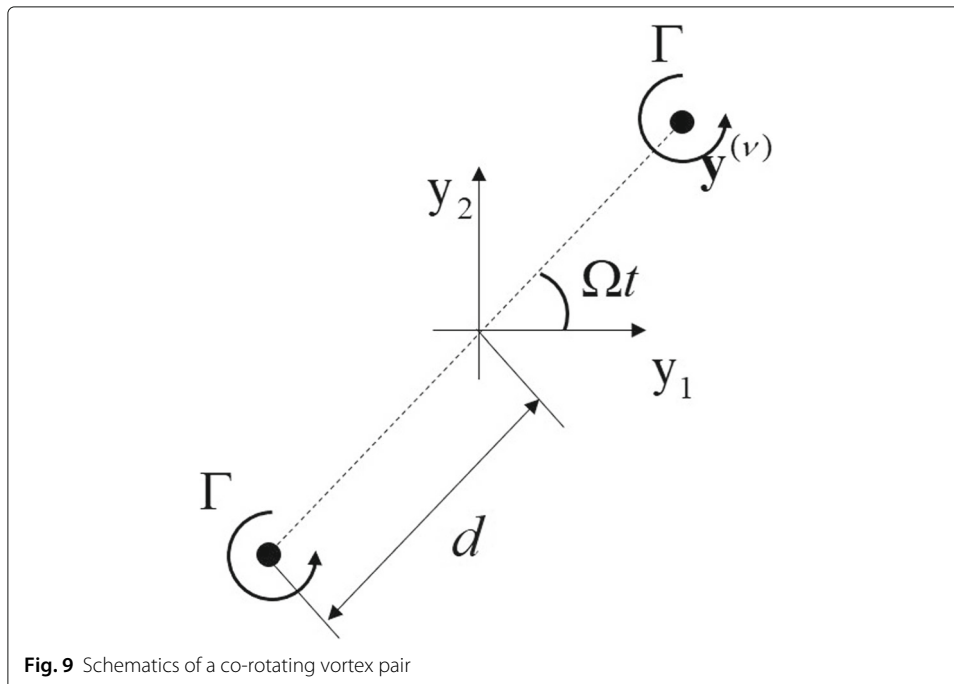

Fig. 9 Schematics of a co-rotating vortex pair

$$k^2 p' + \frac{\partial^2 p'}{\partial x_i^2} = -\rho_0 \mathcal{F}\left(\frac{\partial(\omega \times \mathbf{v})_i}{\partial x_i}\right), \tag{33}$$

where the operator $\mathcal{F}$ defines the Fourier transform. Although we use Lighthill's equation here, the corresponding Green's function is consistent with Green's function of the FW-H equation without freestream flow. Using Gauss's theorem, the far-field acoustic pressure can be computed by

$$\frac{p'}{\rho_0} = \int_V \mathcal{F}\left((\omega \times \mathbf{v})_i\right) \frac{\partial G_{2D}(\mathbf{x}; \mathbf{y})}{\partial y_i} dV. \tag{34}$$

For a co-rotating vortex pair, the Lamb vector $\omega \times \mathbf{v}$ can be expressed as

$$\omega \times \mathbf{v} = -\Omega \Gamma \mathbf{y}^{(\nu)} \left(\delta\left(y_1 - y_1^{(\nu)}\right) \delta\left(y_2 - y_2^{(\nu)}\right) - \delta\left(y_1 + y_1^{(\nu)}\right) \delta\left(y_2 + y_2^{(\nu)}\right)\right), \tag{35}$$

where $\Omega = \frac{\Gamma}{4\pi d^2}$ is the angular velocity of the vortex pair and $\pm \mathbf{y}^{(\nu)} = \pm(d\cos(\Omega t), d\sin(\Omega t))$ represents the location of the vortex pair. By using the sifting property of the Dirac delta function, the frequency-domain far-field acoustic pressure generated by the vortex pair can be obtained by the acoustic pressure expressed as follows

$$\begin{aligned}\frac{p'}{\rho_0} = &-\mathcal{F}\left(\Omega \Gamma d \cos(\Omega t)\left(\left.\frac{\partial G_{2D}}{\partial y_1}\right|_{\mathbf{y}=\mathbf{y}^{(\nu)}} - \left.\frac{\partial G_{2D}}{\partial y_1}\right|_{\mathbf{y}=-\mathbf{y}^{(\nu)}}\right)\right) \\ &- \mathcal{F}\left(\Omega \Gamma d \sin(\Omega t)\left(\left.\frac{\partial G_{2D}}{\partial y_2}\right|_{\mathbf{y}=\mathbf{y}^{(\nu)}} - \left.\frac{\partial G_{2D}}{\partial y_2}\right|_{\mathbf{y}=-\mathbf{y}^{(\nu)}}\right)\right).\end{aligned} \tag{36}$$

To verify the approximations to the derivatives of Green's function, we first conduct Taylor's expansion for Green's function,

$$G_{2D} = G_0 + \sum_j \frac{1}{j!}\left(y_m \frac{\partial}{\partial y_m}\right)^j G_{2D}(\mathbf{x}; \mathbf{y}). \tag{37}$$

By using the approximations to the derivatives of the Green's function given by Eq. (4), we can approximate the expansion of Green's function as follows

$$G_{2D} = G_0 + \sum_j \frac{1}{j!}\left(y_m \frac{\partial \varphi_0}{\partial y_m}\right)^j G_0, \tag{38}$$

where G_0 and $\frac{\partial \varphi_0}{\partial y_m}$ are Green's function G and space derivatives of the phase function $\frac{\partial \varphi}{\partial y_m}$ at the origin. By replacing the Green's function in Eq. (36) with the approximations in Eq. (38), we can obtain the approximated acoustic pressure as follows

$$\frac{p'}{\rho_0} \approx \sum_{j=1}^n \frac{-\Omega \Gamma G_0}{(j-1)!} \mathcal{F}\left(\left(y_1^{(\nu)} \frac{\partial \varphi_0}{\partial y_1} + y_2^{(\nu)} \frac{\partial \varphi_0}{\partial y_2}\right)^j\right)(1 + (-1)^j). \tag{39}$$

It is noted that the first nonzero term in Eq. (39) is the quadrupole term, confirming that the quadrupole source term dominates the acoustic pressure generated by the co-rotating vortex pair [25].

Figure 10 compares the far-field acoustic pressure computed by using the approximated acoustic pressure formulation Eq. (39) with that computed by the acoustic pressure formulation Eq. (36). For the results reported in Fig. 10, the observer is located at $(\frac{100\Omega}{2\pi}, \frac{100\Omega}{2\pi})$, which is sufficiently far away from the centre of the corotating vortex pair. The fluid density is taken as 1kg/m^3. The speed of sound is set as $c = 100 \text{m/s}$, which is sufficiently large compared to the characteristic velocity of the vortex $U = \Omega d$. The distance between the two vortices is $2d = 0.2m$, and the angular velocity is $\Omega = 2\pi$ rad/s.

Fig. 10 Acoustic pressure computed by using the acoustic pressure formulation (Eq. (36)) and the approximated acoustic pressure formulation (Eq. (39))
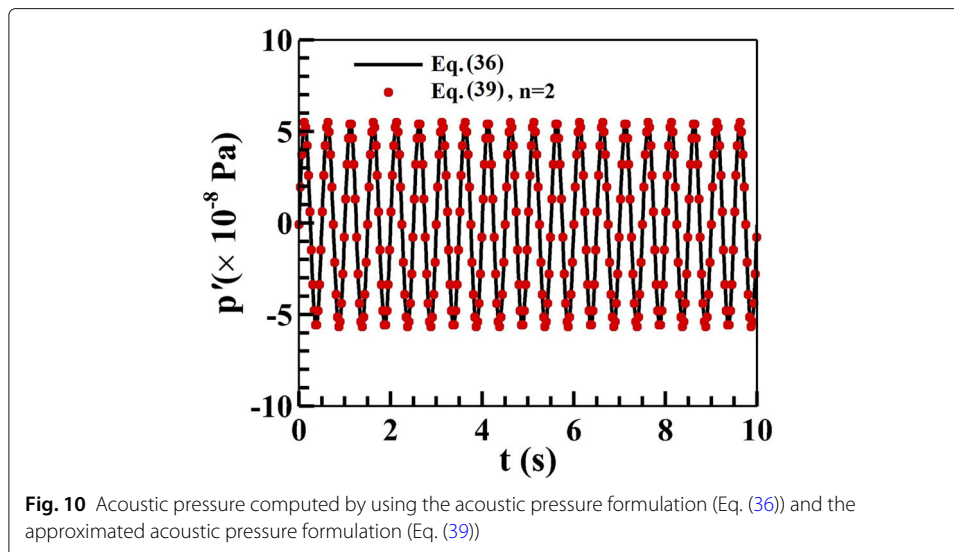
The black solid line in Fig. 10 is the result computed by using the acoustic pressure expression of Eq. (36), while the red circle is computed by using the approximated acoustic pressure formula (Eq. (39) with n=2). It is observed that the approximated acoustic pressure formulation (Eq. (39)) gives a good approximation to the vortex acoustic pressure result (Eq. (36)), indicating that the approximations to the derivatives of Green's function given by Eq. (4) are correct.

4 Conclusion

Computation of the high-order derivatives of Green's function for the FW-H equation is required to eliminate the spurious sound associated with the quadrupole sources. The approximations to the derivatives of Green's function in the frequency domain have been used without derivation in previous work. This work provides the detailed derivations of the approximations to the derivatives of Green's function. The essential expressions and formulations associated with the binomial expression of the derivatives of Green's function and the far-field condition to obtain the approximations are provided in detail. The benchmark flows of the two-dimensional convecting vortex and co-rotating vortex pair are used to verify the approximations. The results show that the approximations can be accurate at different Mach numbers and observer directions as long as the distance is large enough. The derivations of the approximations to integrals of Green's function by using approximations to the derivatives are also reported in detail.

Appendix A: Approximations to the integrals of the Green's function

The approximations to the integrals of Green's function have been used by Zhou et al. [17] to fix the divergence problem of the frequency-domain surface correction integral [20]. However, the detailed derivations of the approximations to the integrals of Green's function have not been provided. In this Appendix, we show that the approximations to the integrals of Green's function can be derived based on the approximations to the derivatives of Green's function.

The approximations to the integrals of Green's function with respect to the variable y_1 at the far field used in the work of Zhou et al. [17] are given as follows

$$\frac{\partial^2 G^{q,n}(\mathbf{x};\mathbf{y})}{\partial y_i \partial y_j} \approx \left(\frac{\partial \varphi(\mathbf{x};\mathbf{y})}{\partial y_q} \right)^{-n} \frac{\partial^2 G(\mathbf{x};\mathbf{y})}{\partial y_i \partial y_j}, \tag{40}$$

where

$$\frac{\partial^2 G^{q,n}(\mathbf{x};\mathbf{y})}{\partial y_i \partial y_j} = I^{q,n} \left(\frac{\partial^2 G(\mathbf{x};\mathbf{y})}{\partial y_i \partial y_j} \right)$$
$$= \int_\infty^{y_q} \left(\int_\infty^{\xi_n} \left(\int_\infty^{\xi_{n-1}} \left(\cdots \int_\infty^{\xi_3} \left(\int_\infty^{\xi_2} K d\xi_1 \right) d\xi_2 \cdots \right) d\xi_{n-2} \right) d\xi_{n-1} \right) d\xi_n,$$
$$K(\mathbf{x};\mathbf{y}) = \frac{\partial^2 G(\mathbf{x};\mathbf{y})}{\partial y_i \partial y_j} \tag{41}$$

is the multiple integral of $\frac{\partial^2 G(\mathbf{x};\mathbf{y})}{\partial y_i \partial y_j}$ with respect to the variable y_q . For the ith integral ($i < n$) from the inner of Eq. (41), the independent variable is ξ_i and the upper limit of the integral is ξ_{i+1}. When $i = n$, the independent variable is ξ_n, and the upper limit of the integral is y_q.

Equation (40) is obtained by proving the following equation

$$\frac{\partial^2 G^{q,l}(\mathbf{x};\mathbf{y})}{\partial y_i \partial y_j} = \frac{\partial^2 \left(\left(\frac{\partial \varphi(\mathbf{x};\mathbf{y})}{\partial y_q} \right)^{-l} G(\mathbf{x};\mathbf{y}) \right)}{\partial y_i \partial y_j}. \tag{42}$$

We give the details of the derivation of Eq. (42) for the two-dimensional flows by using the mathematical induction method and the approximations of Eq. (4). The derivation of Eq. (42) for the three-dimensional flows can be obtained in a similar manner.

To use the mathematical induction method, we first prove that Eq. (42) is valid when $l = 1$ and $q = 1$. For $l = 1$ and $q = 1$, Eq. (41) reduces to

$$\frac{\partial^2 G_{2D}^{1,1}(\mathbf{x};\mathbf{y})}{\partial y_i \partial y_j} = \int_\infty^{y_1} \left(\left. \frac{\partial^2 G_{2D}(\mathbf{x};\mathbf{y})}{\partial y_i \partial y_j} \right|_{y_1=\xi_1} \right) d\xi_1. \tag{43}$$

After transforming the partial derivative with respect to $\mathbf{y}$ to $\mathbf{x}$ and using integration by parts, the right-hand side of Eq. (43) becomes

$$\frac{\partial^2 G_{2D}^{1,1}(\mathbf{x};\mathbf{y})}{\partial y_i \partial y_j} = \frac{\partial^2}{\partial x_i \partial x_j} \int_\infty^{y_1} \frac{i}{4\beta} \left(\frac{2\beta^2}{\pi kR} \right)^{1/2} \exp^{\varphi(\mathbf{x};\xi_1,y_2)} d\xi_1$$
$$= \frac{\partial^2}{\partial x_i \partial x_j} \int_\infty^{y_1} \frac{\partial}{\partial \xi_1} \left[\frac{i}{4\beta} \left(\frac{2\beta^2}{\pi kR} \right)^{1/2} \left(\frac{\partial \varphi(\mathbf{x};\xi_1,y_2)}{\partial \xi_1} \right)^{-1} \exp^{\varphi(\mathbf{x};\xi_1,y_2)} \right] d\xi_1$$
$$- \frac{\partial^2}{\partial x_i \partial x_j} \int_\infty^{y_1} \left[\left(\frac{\partial \varphi(\mathbf{x};\xi_1,y_2)}{\partial \xi_1} \right)^{-1} \exp^{\varphi(\mathbf{x};\xi_1,y_2)} \right] \frac{\partial}{\partial \xi_1} \left(\frac{i}{4\beta} \left(\frac{2\beta^2}{\pi kR} \right)^{1/2} \right) d\xi_1. \tag{44}$$

According to Eq. (16), the integrand in the last term on the right-hand side of Eq. (44) is of order $O(R^{-3/2})$. Meanwhile, the left-hand side of Eq. (44) is of order $O(R^{-1/2})$. Thus, the last term on the right-hand side of Eq. (44) can be neglected compared with the left-hand side of Eq. (44), so that we have

$$\frac{\partial^2 G_{2D}^{1,1}(\mathbf{x};\mathbf{y})}{\partial y_i \partial y_j} \approx \frac{\partial^2}{\partial x_i \partial x_j} \int_\infty^{y_1} \frac{\partial}{\partial \xi_1} \left[\frac{i}{4\beta} \left(\frac{2\beta^2}{\pi kR} \right)^{1/2} \left(\frac{\partial \varphi(\mathbf{x};\xi_1,y_2)}{\partial \xi_1} \right)^{-1} \exp^{\varphi(\mathbf{x};\xi_1,y_2)} \right] d\xi_1. \tag{45}$$

Considering the limit of Green's function at infinity and transforming the partial derivative with respect to **x** back to **y**, Eq. (45) becomes

$$\begin{aligned}
\frac{\partial^2 G_{2D}^{1,1}(\mathbf{x};\mathbf{y})}{\partial y_i \partial y_j} &\approx \frac{\partial^2}{\partial y_i \partial y_j} \left[\frac{i}{4\beta} \left(\frac{2\beta^2}{\pi kR} \right)^{1/2} \left(\frac{\partial \varphi(\mathbf{x};\mathbf{y})}{\partial y_1} \right)^{-1} \exp^{\varphi(\mathbf{x};\mathbf{y})} \right] \\
&= \frac{\partial^2 \left(\left(\frac{\partial \varphi(\mathbf{x};\mathbf{y})}{\partial y_1} \right)^{-1} G_{2D}(\mathbf{x};\mathbf{y}) \right)}{\partial y_i \partial y_j},
\end{aligned} \tag{46}$$

proving that Eq. (42) is valid when $l = 1$ and $q = 1$.

According to the procedures of the mathematical induction method, we assume that Eq. (42) is valid when $l = h$ and $q = 1$.

$$\frac{\partial^2 G_{2D}^{1,h}(\mathbf{x};\mathbf{y})}{\partial y_i \partial y_j} \approx \frac{\partial^2 \left[\left(\frac{\partial \varphi(\mathbf{x};\mathbf{y})}{\partial y_1} \right)^{-h} G_{2D}(\mathbf{x};\mathbf{y}) \right]}{\partial y_i \partial y_j}. \tag{47}$$

According to Eqs. (41) and (47), we have

$$\frac{\partial^2 G_{2D}^{1,h+1}(\mathbf{x};\mathbf{y})}{\partial y_i \partial y_j} \approx \int_\infty^{y_h} \left(\frac{\partial^2 \left[\left(\frac{\partial \varphi(\mathbf{x};\mathbf{y})}{\partial y_1} \right)^{-l} G_{2D}(\mathbf{x};\mathbf{y}) \right]}{\partial y_i \partial y_j} \Bigg|_{y_1=\xi_1} \right) d\xi_1. \tag{48}$$

Using integration by parts, we reformulate Eq. (48) as follows

$$\begin{aligned}
\frac{\partial^2 G_{2D}^{1,h+1}(\mathbf{x};\mathbf{y})}{\partial y_i \partial y_j} &\approx \frac{\partial^2}{\partial x_i \partial x_j} \int_\infty^{y_1} \left(\frac{i}{4\beta} \left(\frac{\partial \varphi(\mathbf{x};\mathbf{y})}{\partial y_1} \right)^{-h} \left(\frac{2\beta^2}{\pi kR} \right)^{1/2} \exp^{\varphi(\mathbf{x};\mathbf{y})} \Bigg|_{y_1=\xi_1} \right) d\xi_1 \\
&= \frac{\partial^2}{\partial x_i \partial x_j} \int_\infty^{y_1} \left\{ \frac{\partial}{\partial y_1} \left[\frac{i}{4\beta} \left(\frac{\partial \varphi(\mathbf{x};\mathbf{y})}{\partial y_1} \right)^{-h} \left(\frac{2\beta^2}{\pi kR} \right)^{1/2} \left(\frac{\partial \varphi(\mathbf{x};\mathbf{y})}{\partial y_1} \right)^{-1} \exp^{\varphi(\mathbf{x};\mathbf{y})} \right] \Bigg|_{y_1=\xi_1} \right\} d\xi_1 \\
&\quad - \frac{\partial^2}{\partial x_i \partial x_j} \int_\infty^{y_1} \left\{ \left[\left(\frac{\partial \varphi(\mathbf{x};\mathbf{y})}{\partial y_1} \right)^{-1} \exp^{\varphi(\mathbf{x};\mathbf{y})} \right] \frac{\partial}{\partial y_1} \left[\frac{i}{4\beta} \left(\frac{\partial \varphi(\mathbf{x};\mathbf{y})}{\partial y_1} \right)^{-h} \left(\frac{2\beta^2}{\pi kR} \right)^{1/2} \right] \Bigg|_{y_1=\xi_1} \right\} d\xi_1.
\end{aligned} \tag{49}$$

From Eq. (16), we know that the last term on the right-hand side of Eq. (49) can be neglected compared with the left-hand side of Eq. (49). Similar to the derivation of Eq. (46), Eq. (49) can be approximated by

$$\frac{\partial^2 G_{2D}^{1,h+1}(\mathbf{x};\mathbf{y})}{\partial y_i \partial y_j} \approx \frac{\partial^2}{\partial y_i \partial y_j} \left[\frac{i}{4\beta} \left(\frac{2\beta^2}{\pi kR} \right)^{1/2} \left(\frac{\partial \varphi(\mathbf{x};\mathbf{y})}{\partial y_1} \right)^{-(h+1)} \exp^{\varphi(\mathbf{x};\mathbf{y})} \right]. \tag{50}$$

Equation (50) shows that Eq. (42) is valid when $l = h + 1$ and $q = 1$.

By using the Leibniz product rule, the right-hand side of Eq. (42) is equal to

$$
\frac{\partial^2}{\partial y_i \partial y_j} \left[\frac{i}{4\beta} \left(\frac{2\beta^2}{\pi k} \right)^{1/2} \left(R^{-1/2} \left(\frac{\partial \varphi(\mathbf{x}; \mathbf{y})}{\partial y_1} \right)^{-l} \right) \exp^{\varphi(\mathbf{x};\mathbf{y})} \right]
$$

$$
= \frac{i}{4\beta} \left(\frac{2\beta^2}{\pi k} \right)^{1/2} \left[R^{-1/2} \left(\frac{\partial \varphi(\mathbf{x}; \mathbf{y})}{\partial y_1} \right)^{-l} \exp^{\varphi(\mathbf{x};\mathbf{y})} \left(\left(\frac{\partial \varphi(\mathbf{x}; \mathbf{y})}{\partial y_i} \right) \left(\frac{\partial \varphi(\mathbf{x}; \mathbf{y})}{\partial y_j} \right) + o(1) \right) \right]
$$

$$
+ \frac{i}{4\beta} \left(\frac{2\beta^2}{\pi k} \right)^{1/2} \left[\frac{\partial \left(R^{-1/2} \left(\frac{\partial \varphi(\mathbf{x};\mathbf{y})}{\partial y_1} \right)^{-l} \right)}{\partial y_i} \frac{\partial \left(\exp^{\varphi(\mathbf{x};\mathbf{y})} \right)}{\partial y_j} \right]
$$

$$
+ \frac{i}{4\beta} \left(\frac{2\beta^2}{\pi k} \right)^{1/2} \left[\frac{\partial \left(R^{-1/2} \left(\frac{\partial \varphi(\mathbf{x};\mathbf{y})}{\partial y_1} \right)^{-l} \right)}{\partial y_j} \frac{\partial \left(\exp^{\varphi(\mathbf{x};\mathbf{y})} \right)}{\partial y_i} \right]
$$

$$
+ \frac{i}{4\beta} \left(\frac{2\beta^2}{\pi k} \right)^{1/2} \left[\frac{\partial^2 \left(R^{-1/2} \left(\frac{\partial \varphi(\mathbf{x};\mathbf{y})}{\partial y_1} \right)^{-l} \right)}{\partial y_i \partial y_j} \exp^{\varphi(\mathbf{x};\mathbf{y})} \right].
$$

(51)

In the far field, $\frac{\partial \varphi(\mathbf{x};\mathbf{y})}{\partial y_i}$ is of order $O(1)$, and the derivative of $R^{-1/2} \left(\frac{\partial \varphi(\mathbf{x};\mathbf{y})}{\partial y_1} \right)^{-l}$ can be expressed by $o\left(R^{-1/2} \left(\frac{\partial \varphi(\mathbf{x};\mathbf{y})}{\partial y_1} \right)^{-l} \right)$. Thus, the last three terms of Eq. (51) can be neglected compared with the first term on the right-hand side. We ignore the derivatives corresponding to $\left(\frac{\partial \varphi(\mathbf{x};\mathbf{y})}{\partial y_1} \right)^{-l}$ and obtain

$$
\frac{\partial^2}{\partial y_i \partial y_j} \left[\frac{i}{4\beta} \left(\frac{2\beta^2}{\pi k} \right)^{1/2} \left(R^{-1/2} \left(\frac{\partial \varphi(\mathbf{x}; \mathbf{y})}{\partial y_1} \right)^{-l} \right) \exp^{\varphi(\mathbf{x};\mathbf{y})} \right]
$$

$$
\approx \left(\frac{\partial \varphi(\mathbf{x}; \mathbf{y})}{\partial y_1} \right)^{-l} \frac{\partial^2}{\partial y_i \partial y_j} \left[\frac{i}{4\beta} \left(\frac{2\beta^2}{\pi k} \right)^{1/2} R^{-1/2} \exp^{\varphi(\mathbf{x};\mathbf{y})} \right]
$$

$$
= \left(\frac{\partial \varphi(\mathbf{x}; \mathbf{y})}{\partial y_1} \right)^{-l} \frac{\partial^2 G_{2D}}{\partial y_i \partial y_j}.
$$

(52)

Finally, substituting Eq. (52) in Eq. (50) yields Eq. (40). Thus, approximations to the integral of Green's function are derived.

We use a homogeneous vortical flow with a uniform Lighthill stress tensor to verify the far-field approximations to the integrals of Green's function. We define the uniform Lighthill stress tensor as $T_{ij} = A \cos(2\pi ft)$, where A is $1/s^2$. The uniform vortical flow moves within a domain V of $[0, 10] \times [0, 10]$. The frequency f is taken as 1Hz. The speed of sound is taken as $c_0 = 340$m/s, and the density is taken as $\rho = 1$kg/m^3. The far-field observer is located at $(340000\text{m}, 340000\text{m})$, which is sufficiently large compared to the wavelength of sound. The freestream Mach number is 0.3 along the $o - y_1$ axis. The contribution from the Lighthill stress tensor to the far-field sound can be computed by using the quadrupole source term in the FW-H integral as follows

$$
I_{Q,\text{FW}-\text{H}} = \int_V T_{ij} \frac{\partial^2 G_{2D}(\mathbf{x}; \mathbf{y})}{\partial y_i \partial y_j} \mathrm{d}\mathbf{y}.
$$

(53)

By using the far-field approximations to the integrals of Green's function (Eq. (40)), the far-field sound can be approximated by

$$
\begin{aligned}
I_{Q,\mathrm{appr}} &= T_{ij} \int_V \frac{\partial^2 G_{2D}(\mathbf{x};\mathbf{y})}{\partial y_i \partial y_j} \mathrm{d}\mathbf{y} \\
&= \frac{1}{2} T_{ij} \int_V \frac{\partial}{\partial y_1}\left(\left(\frac{\partial \varphi_{2D}}{\partial y_1}\right)^{-1} \frac{\partial^2 G_{2D}(\mathbf{x};\mathbf{y})}{\partial y_i \partial y_j}\right) + \frac{\partial}{\partial y_2}\left(\left(\frac{\partial \varphi_{2D}}{\partial y_2}\right)^{-1} \frac{\partial^2 G_{2D}(\mathbf{x};\mathbf{y})}{\partial y_i \partial y_j}\right) \mathrm{d}\mathbf{y} \\
&= \frac{1}{2} T_{ij} \int_S \left(\frac{\partial \varphi_{2D}}{\partial y_q}\right)^{-1} \frac{\partial^2 G_{2D}(\mathbf{x};\mathbf{y})}{\partial y_i \partial y_j} n_q \mathrm{d}\mathbf{y}.
\end{aligned}
$$

$$(54)$$

Figure 11 shows the results calculated by using Eqs. (53) and (54), respectively. The results computed by using the surface integral (Eq. (54)) match well with the volume integral (Eq. (53)), indicating that the approximation to the integrals of Green's function is valid.

Appendix B: Derivation of Eqs. (15) and (16)

The detailed derivation of Eqs. (15) and (16) in Section 2.2 are given in this Appendix. Here, we start from the derivation of Eq. (15).

According to Eqs. (7) and (10), we rewrite R as

$$
\begin{aligned}
R &= \left(g_l r_l^2\right)^{1/2}, \\
g_l &= 1 + \left(\beta^2 - 1\right)\left(1 - \delta_{1l}\right), \\
r_l &= y_l - x_l,
\end{aligned}
$$

$$(55)$$

where the subscript $l = 1, 2$ in two dimension and $l = 1, 2, 3$ in three dimension. The Einstein summation convention is used in Eq. (55). $\beta = \sqrt{1 - M^2}$ is the Prantle-Glauert factor. M is the Mach number of the freestream flow. δ_{ij} is the Kronecker delta function.
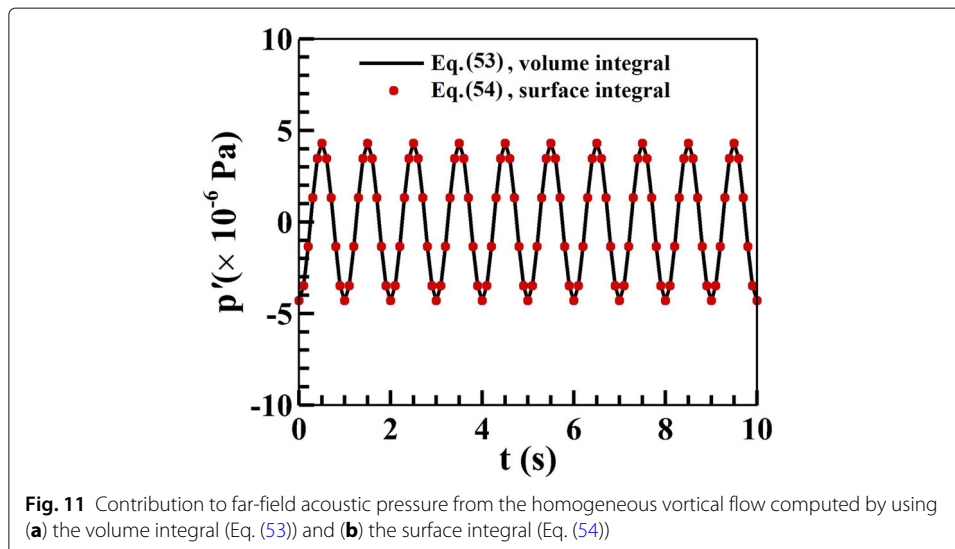

Fig. 11 Contribution to far-field acoustic pressure from the homogeneous vortical flow computed by using (**a**) the volume integral (Eq. (53)) and (**b**) the surface integral (Eq. (54))

By defining $\lambda_1 = g_1^{1/2} r_1$, the 1st- to 3rd-order derivatives of the distance R can be reformulated as follows

$$\frac{\partial R}{\partial y_1} = \frac{\partial R}{\partial \lambda_1} \frac{\partial \lambda_1}{\partial y_1} = g_l^{1/2} \frac{\partial R}{\partial \lambda_1}, \tag{56}$$

$$\frac{\partial^2 R}{\partial y_1^2} = \frac{\partial}{\partial \lambda_1} \left(\frac{\partial R}{\partial y_1} \right) \frac{\partial \lambda_1}{\partial y_1} = \frac{\partial}{\partial \lambda_1} \left(g_l^{1/2} \frac{\partial R}{\partial \lambda_1} \right) \frac{\partial \lambda_1}{\partial y_1} = g_l \frac{\partial^2 R}{\partial \lambda_1^2}, \tag{57}$$

$$\frac{\partial^3 R}{\partial y_1^3} = \frac{\partial}{\partial \lambda_1} \left(\frac{\partial^2 R}{\partial y_1^2} \right) \frac{\partial \lambda_1}{\partial y_1} = \frac{\partial}{\partial \lambda_1} \left(g_l \frac{\partial^2 R}{\partial \lambda_1^2} \right) \frac{\partial \lambda_1}{\partial y_1} = g_l^{3/2} \frac{\partial^3 R}{\partial \lambda_1^3}. \tag{58}$$

For the high-order derivatives of the distance R, we have

$$\frac{\partial^{k_1} R}{\partial y_1^{k_1}} = g_l^{k_1/2} \frac{\partial^{k_1} R}{\partial \lambda_1^{k_1}}. \tag{59}$$

We can estimate that $g_l \sim O(1)$, since $0 \leq \beta < 1$, $max(\delta_{1l}) = 1$, and $min(\delta_{1l}) = 0$. For the computation of far-field sound, we approximately estimate the order of magnitude by using the assumption $\lambda_1 \sim O(R)$. We notice that this assumption is not true for the observer near the vertical direction. However, it gives a reasonable approximation to the order of magnitude for the observer at the most part of the region. The numerical result in Section 3 also shows that the above relations give good approximations to the far-field sound pressure. The detailed investigation to the effects of this assumption on the results is expected to be conducted in the future.

We denote R as $DR^{m_1} \lambda_1^{n_1}$ with $D = 1$, $m_1 = 1$ and $n_1 = 0$. Further, the derivative of $R^{m_1} \lambda_1^{n_1}$ with respect to λ_1 is $m_1 R^{m_1-2} \lambda_1^{n_1+1} + n_1 R^{m_1} \lambda_1^{n_1-1}$. $R^{m_1} \lambda_1^{n_1}$ and $m_1 R^{m_1-2} \lambda_1^{n_1+1} + n_1 R^{m_1} \lambda_1^{n_1-1}$ are of the order $O(R^{m_1+n_1})$ and $O(R^{m_1+n_1-1})$, respectively. In the most part of the region where $\lambda_1 \sim O(R)$, the derivative of $R^{m_1} \lambda_1^{n_1}$ with respect to λ_1 is one order smaller than $R^{m_1} \lambda_1^{n_1}$. Therefore, the k_1-th order derivative of R with respect to λ_1 is of the order $O(R^{1-k_1})$. According to Eq. (59), $\frac{\partial^{k_1} R}{\partial y_1^{k_1}}$ is thus of the order $O(R^{1-k_1})$. Therefore, we can express the k_1th-order derivative of R with respect to y_1 as

$$\frac{\partial^{k_1} R}{\partial y_1^{k_1}} \approx O\left(R^{-k_1} \right) R. \tag{60}$$

It is noted that the first order derivative of R with respect to y_1 is $\frac{\partial R}{\partial y_1} = \frac{\lambda_1}{R} g_l^{1/2} \sim O(1)$ in the most part of the region where $\lambda_1 \sim O(R)$. For Eq. (16), a similar formulation to the Eq. (63) can be obtained as follows

$$\frac{\partial^{k_1} R^{-1/2}}{\partial y_1^{k_1}} = \frac{\partial^{k_1} R^{-1/2}}{\partial \lambda_1^{k_1}} g_l^{k_1/2}. \tag{61}$$

The derivation of Eq. (61) can be obtained by a similar way to that of Eq. (59) with the use of chain rule. It is noted that $R^{-1/2}$ can be written as $DR^{m_1} \lambda_1^{n_1}$ with $D = 1$, $m_1 = -1/2$ and $n_1 = 0$. The derivative of $R^{m_1} \lambda_1^{n_1}$ with respect to λ_1 is $m_1 R^{m_1-2} \lambda_1^{n_1+1} + n_1 R^{m_1} \lambda_1^{n_1-1}$. $R^{m_1} \lambda_1^{n_1}$ and $m_1 R^{m_1-2} \lambda_1^{n_1+1} + n_1 R^{m_1} \lambda_1^{n_1-1}$ are of the order $O(R^{m_1+n_1})$ and $O(R^{m_1+n_1-1})$, respectively. In the most part of the region where $\lambda_1 \sim O(R)$, the derivative of $R^{m_1} \lambda_1^{n_1}$ with respect to λ_1 is one order smaller than $R^{m_1} \lambda_1^{n_1}$. Therefore, the k_1th-order derivative of $R^{-1/2}$ with respect to λ_1 is of the order $O(R^{-1/2-k_1})$. According to Eq. (61), $\frac{\partial^{k_1} R^{-1/2}}{\partial y_1^{k_1}}$ is thus of the order $O(R^{-1/2-k_1})$. Therefore, we can express the k_1-th order

derivative of R with respect to y_1 as

$$\frac{\partial^{k_1} R^{-1/2}}{\partial y_1^{k_1}} \approx O\left(R^{-k_1}\right) R^{-1/2}. \tag{62}$$

Appendix C: Derivation of Eq. (17)

The detailed derivation of Eq. (17) is reported in this Appendix. We expand the k_1 th-order derivative of $\exp^\varphi$ as follows

$$\begin{aligned}
\frac{\partial^{k_1}}{\partial y_1^{k_1}} \exp^\varphi &= \left(\frac{\partial \varphi}{\partial y_1}\right)^{k_1} \exp^\varphi + E_1 \left(\frac{\partial \varphi}{\partial y_1}\right)^{k_1-1} \frac{\partial^2 \varphi}{\partial y_1^2} \exp^\varphi \\
&\quad + E_2 \left(\frac{\partial \varphi}{\partial y_1}\right)^{k_1-2} \frac{\partial^3 \varphi}{\partial y_1^3} \exp^\varphi + E_3 \left(\frac{\partial \varphi}{\partial y_1}\right)^{k_1-3} \frac{\partial^4 \varphi}{\partial y_1^4} \exp^\varphi \\
&\quad + E_4 \left(\frac{\partial \varphi}{\partial y_1}\right)^{k_1-4} \left(\frac{\partial^2 \varphi}{\partial y_1^2}\right)^2 \exp^\varphi + ...,
\end{aligned} \tag{63}$$

where E_1, E_2, E_3, E_4... are the coefficients corresponding to the number of derivative's order k_1.

We start from the derivation from the Eq. (17) in the two-dimensional space. According to Eq. (6), the exponent φ of the 2D Green's function for the FW-H equation is as follows

$$\varphi(\mathbf{x}; \mathbf{y}) = \mathrm{i} \left[\frac{Mk(x_1 - y_1)}{\beta^2} + \frac{\pi}{4} - \frac{k}{\beta^2} R \right], \quad R = \sqrt{(x_1 - y_1)^2 + \beta^2 (x_1 - y_1)^2}, \tag{64}$$

where $\mathrm{i} = \sqrt{-1}$ is the unit of the imaginary number. $k = \omega/c_o$ is the acoustic wavenumber where ω and c_o are the angular frequency and the speed of sound, respectively. $\mathbf{x}$ and $\mathbf{y}$ are the coordinate of observer and source locations, respectively. $\beta = \sqrt{1 - M^2}$ is the Prantle-Glauert factor. M is the Mach number of the freestream flow.

The derivative of the exponent φ with respect to y_1 is

$$\frac{\partial \varphi}{\partial y_1} = \frac{-\mathrm{i}Mk}{\beta^2} - \frac{\mathrm{i}k}{\beta^2} \frac{\partial R}{\partial y_1}. \tag{65}$$

The k_1th-order ($k_1 \geq 2$) derivative of φ with respect to y_1 is

$$\frac{\partial^{k_1} \varphi}{\partial y_1^{k_1}} = \frac{-\mathrm{i}k}{\beta^2} \frac{\partial^{k_1} R}{\partial y_1^{k_1}}. \tag{66}$$

When $\frac{\partial^{k_1} \varphi}{\partial y_1^{k_1}} = 0$ ($k_1 \geq 2$), Eq. (63) reduces to

$$\frac{\partial^{k_1} \exp^{\varphi(\mathbf{x};\mathbf{y})}}{\partial y_1^{k_1}} = \left(\frac{\partial \varphi(\mathbf{x}; \mathbf{y})}{\partial y_1}\right)^{k_1} \exp^{\varphi(\mathbf{x};\mathbf{y})}. \tag{67}$$

When $\frac{\partial^{k_1} \varphi}{\partial y_1^{k_1}} \neq 0$ ($k_1 \geq 2$), the ratio between $\frac{\partial \varphi}{\partial y_1}$ and $\frac{\partial^{k_1} \varphi}{\partial y_1^{k_1}}$ ($k_1 \geq 2$) is

$$\frac{\frac{\partial \varphi}{\partial y_1}}{\frac{\partial^{k_1} \varphi}{\partial y_1^{k_1}}} = \frac{M + \frac{\partial R}{\partial y_1}}{\frac{\partial^{k_1} R}{\partial y_1^{k_1}}}. \tag{68}$$

For subsonic flows with $0 \leq M < 1$, we have $\frac{\partial \varphi}{\partial y_1} / \frac{\partial^{k_1} \varphi}{\partial y_1^{k_1}} \sim O(R^{k_1-1})$ according to Eq. (60), which means that $\frac{\partial \varphi}{\partial y_1}$ is much larger than $\frac{\partial^{k_1} \varphi}{\partial y_1^{k_1}}$ ($k_1 \geq 2$) at the far-field ($R \gg 1$).

It is noticed that E_1, E_2, E_3, E_4... in Eq. (63) are dependent on the order of the derivative k_1 and independent of the distance R. For the computation of sound at far field, we can always find large enough distance R which is much larger than the coefficients E_1, E_2, E_3, E_4.... Therefore, by ignoring the terms including high order derivatives of $\exp^\varphi$ in Eq. (63), Eq. (63) can be approximately computed as follows,

$$\frac{\partial^{k_1} \exp^{\varphi(\mathbf{x};\mathbf{y})}}{\partial y_1^{k_1}} \approx \left(\frac{\partial \varphi(\mathbf{x};\mathbf{y})}{\partial y_1} \right)^{k_1} \exp^{\varphi(\mathbf{x};\mathbf{y})}. \tag{69}$$

Equation (17) in Section 2 can be obtained by combining Eqs. (67) and (69). The derivation of Eq. (17) for in three-dimensional space can be obtained in a similar way.

Authors' contributions
Zhiteng Zhou provided the derivation and wrote the manuscript. Zhengyu Zang examined and revised the derivation with benchmarks. Hongping Wang read and revised the format of equations. Shizhao Wang revised the derivation and the manuscript. All authors read and approved the final manuscript.

Declarations

Competing interests
The authors declare that they have no competing interests.

Author details
[1]Institute of Mechanics, Chinese Academy of Sciences, 100190 Beijing, China. [2]School of Engineering Sciences, University of Chinese Academy of Sciences, 100049 Beijing, China.

References
1. Williams JEF, Hawkings DL (1969) Sound generation by turbulence and surfaces in arbitrary motion. Philos Trans R Soc A 264(1151):321–342
2. Pouangué AF, Sanjosé M, Moreau S, Daviller G, Deniau H (2015) Subsonic jet noise simulations using both structured and unstructured grids. AIAA J 53(1):55–69
3. Shur ML, Spalart PR, Strelets MK, Travin AK (2003) Towards the prediction of noise from jet engines. Int J Heat Fluid Flow 24(4):551–561
4. Poggi C, Rossetti M, Bernardini G, Iemma U, Andolfi C, Milano C, Gennaretti M (2021) Surrogate models for predicting noise emission and aerodynamic performance of propellers. Aerosp Sci Technol (in press). https://doi.org/10.1016/j.ast.2021.107016
5. Li F, Huang Q, Pan G, Shi Y (2021) Numerical study on hydrodynamic performance and flow noise of a hydrofoil with wavy leading-edge. AIP Adv 11(9):095105
6. Sun Z, Song J, An Y (2012) Numerical simulation of aerodynamic noise generated by high speed trains. Eng Appl Comput Fluid Mech 6(2):173–185
7. Mo H, An Y, Liu Q (2019) Influence of the length of high-speed train on the far-field aeroacoustics characteristics. Chin J Theor Appl Mech 51(5):1310–1320
8. Song H, Yi M, Huang J, Pan Y, Liu D (2016) Numerical method to compute acoustic scattering effect of a moving source. SpringerPlus 5:1404
9. Zhang Y, Meng W, Fan B, Tang W (2016) Biomimetic optimization research on wind noise reduction of an asymmetric cross-section bar. SpringerPlus 5:1221
10. Lockard DP (2000) An efficient, two-dimensional implementation of the Ffowcs Williams and Hawkings equation. J Sound Vib 229(4):897–911
11. Glegg S, Devenport W (2017) Aeroacoustics of low mach number flows: fundamentals, analysis, and measurement. Academic Press, Oxford
12. Farassat F (2007) Derivation of Formulations 1 and 1A of Farassat. NASA Technical Memorandum NASA/TM-2007-214853

13. Ikeda T, Enomoto S, Yamamoto K, Amemiya K (2013) On the modification of the Ffowcs Williams-Hawkings integration for jet noise prediction. Paper presented at the 19th AIAA/CEAS aeroacoustics conference, AIAA 2013-2277, Berlin, 27-29 May 2013
14. Yao H-D, Davidson L, Eriksson L-E (2017) Noise radiated by low-Reynolds number flows past a hemisphere at $Ma = 0.3$. Phys Fluids 29(7):076102
15. Zhong S, Zhang X (2018) On the frequency domain formulation of the generalized sound extrapolation method. J Acoust Soc Am 144(1):24–31
16. Zhong S, Zhang X (2017) A sound extrapolation method for aeroacoustics far-field prediction in presence of vortical waves. J Fluid Mech 820:424–450
17. Zhou Z, Wang H, Wang S, He G (2021) Lighthill stress flux model for Ffowcs Williams–Hawkings integrals in frequency domain. AIAA J 59(11):4809–4814
18. Nitzkorski Z, Mahesh K (2014) A dynamic end cap technique for sound computation using the Ffowcs Williams and Hawkings equations. Phys Fluids 26(11):115101
19. Wang M, Lele SK, Moin P (1996) Computation of quadrupole noise using acoustic analogy. AIAA J 34(11):2247–2254
20. Lockard D, Casper J (2005) Permeable surface corrections for Ffowcs Williams and Hawkings integrals. Paper presented at the 11th AIAA/CEAS aeroacoustics conference, AIAA 2005-2995, Monterey, 23-25 May 2005
21. Zhou Z, Wang H, Wang S (2021) Simplified permeable surface correction for frequency-domain Ffowcs Williams and Hawkings integrals. Theor Appl Mech Lett 11(4):100259
22. Feng F, Meng X, Wang Q (2020) Sound generation by a pair of co-rotating vortices using spectral acoustic analogy. J Sound Vib 469:115120
23. Leweke T, Le Dizès S, Williamson CHK (2016) Dynamics and instabilities of vortex pairs. Annu Rev Fluid Mech 48:507–541
24. Howe MS (2002) Theory of Vortex Sound. Cambridge University Press, Cambridge
25. Mitchell BE, Lele SK, Moin P (1995) Direct computation of the sound from a compressible co-rotating vortex pair. J Fluid Mech 285:181–202

Publisher's Note